



Photosynthesis-assisted remodeling of three-dimensional printed structures

Kunhao Yu^{a,1}, Zhangzhengrong Feng^{a,1}, Haixu Du^a, An Xin^a, Kyung Hoon Lee^a, Ketian Li^a, Yipin Su^a, Qiming Wang^{a,2}, Nicholas X. Fang^{b,2}, and Chiara Daraio^{c,2}

^aSonny Astani Department of Civil and Environmental Engineering, University of Southern California, Los Angeles, CA 90089; ^bDepartment of Mechanical Engineering, Massachusetts Institute of Technology, Cambridge, MA 02139; and ^cDivision of Engineering and Applied Science, California Institute of Technology, Pasadena, CA 91125

Edited by Zhigang Suo, Harvard University, Cambridge, MA, and approved December 10, 2020 (received for review August 4, 2020)

The mechanical properties of engineering structures continuously weaken during service life because of material fatigue or degradation. By contrast, living organisms are able to strengthen their mechanical properties by regenerating parts of their structures. For example, plants strengthen their cell structures by transforming photosynthesis-produced glucose into stiff polysaccharides. In this work, we realize hybrid materials that use photosynthesis of embedded chloroplasts to remodel their microstructures. These materials can be used to three-dimensionally (3D)-print functional structures, which are endowed with matrix-strengthening and crack healing when exposed to white light. The mechanism relies on a 3D-printable polymer that allows for an additional cross-linking reaction with photosynthesis-produced glucose in the material bulk or on the interface. The remodeling behavior can be suspended by freezing chloroplasts, regulated by mechanical preloads, and reversed by environmental cues. This work opens the door for the design of hybrid synthetic-living materials, for applications such as smart composites, lightweight structures, and soft robotics.

3D printing | self-remodeling | self-strengthening | self-healing | photosynthesis

Plants can grow and form complex, hierarchical structures that are challenging to reproduce with traditional engineering practices (1). Plant cells use photosynthesis to produce glucose, which is delivered to selected locations, such as trunks and crotches. Glucose, in turn, is used to form stiff polysaccharides (e.g., cellulose, chitosan, and chitin), which remodel and strengthen the plant structures locally (Fig. 1*A*) (2, 3). For example, the stiffness of a young stem is typically on the order of kilopascal, while the stiffness of a mature trunk can reach as high as several gigapascals (4). Mechanical loads are found to augment the strengthening of the plant structure through mechanotransduction pathways (5). In recent years, the availability of three-dimensional (3D)-printing technologies has driven the fabrication of engineering structures that attempt to mimic the complexity of the plants' architectures (6–10). However, how to mimic the plants' ability to remodel their components and strengthen mechanical properties remains elusive. Synthetic structures, on the contrary, typically weaken during service life because of materials fatigue or degradation. Developing hybrid, 3D-printable materials that exploit living photosynthesis processes to remodel their structures would be a major leap forward in engineering materials that mimic natural systems. However, establishing a communication channel between the synthetic 3D-printable materials and the natural photosynthesis process is challenging.

Here, we present a class of 3D-printable polymers that can be remodeled by the photosynthesis of embedded chloroplasts to enable matrix strengthening and crack healing. With local light exposure, the polymers harness photosynthesis-produced glucose to facilitate an additional cross-linking reaction, forming a stiff region with “artificial polysaccharides” (Fig. 1*B*). The region with additional cross-links features enhanced Young's modulus, tensile strength, and fracture toughness by factors of 300–620%,

compared to the region without the additional cross-links. Such photosynthesis-assisted strengthening can be suspended by freezing living chloroplasts, regulated by external mechanical preloads, and reversed by cleaving glucose cross-linkers with environmental cues. We also show that the photosynthesis-assisted strengthening can be applied to 3D-printed structures through patterned light and patterned loads. In addition, the photosynthesis can equip the 3D-printed structures with a healing capability via glucose-enabled interfacial cross-linking. The paradigm in this work provides a unique platform for remodeling engineering materials via the communication between synthetic polymers and natural photosynthesis processes.

Mechanism of Photosynthesis-Assisted Strengthening

To design a polymer network that allows for an additional cross-linking reaction with the photosynthesis-produced glucose, we design a polymer resin that features both acrylate and isocyanate distal groups (NCO) and then blend the resin with chloroplasts extracted from spinach leaves (*SI Appendix, Figs. S1 and S2*) (11). The acrylate groups can be utilized for the photopolymerization-based 3D printing (such as stereolithography), because the acrylate groups allow for a photoinitiated addition reaction to polymerize the resin (*SI Appendix, Fig. S3*) (12, 13). The printing is rapid with a speed of 75–400 $\mu\text{m/s}$, and the resolution can reach as

Significance

Living creatures are continuous sources of inspiration for designing engineering materials and structures. However, synthetic engineering materials are typically different from living creatures, because the latter consist of living cells to support their metabolisms, such as remodeling, growth, and reproduction. How to harness living cells to metabolize synthetic engineering materials remains largely elusive. Here, we report an attempt to exploit living chloroplasts to metabolize three-dimensional-printed polymers. With living chloroplasts and synthetic polymers, the system leads to a class of hybrid synthetic-living materials whose microstructures and properties can be remodeled on-demand by the photosynthesis of chloroplasts.

Author contributions: K.Y., Z.F., Q.W., N.X.F., and C.D. designed research; K.Y., Z.F., H.D., A.X., K.H.L., K.L., Y.S., and Q.W. performed research; K.Y., Z.F., H.D., A.X., K.H.L., K.L., Y.S., and Q.W. contributed new reagents/analytic tools; K.Y., Z.F., Q.W., N.X.F., and C.D. analyzed data; K.Y., Z.F., H.D., A.X., K.H.L., K.L., Y.S., Q.W., N.X.F., and C.D. wrote the paper; and Q.W. conceived the idea and supervised the team.

Competing interest statement: The University of Southern California has filed a patent application related to the work described here.

This article is a PNAS Direct Submission.

Published under the PNAS license.

¹K.Y. and Z.F. contributed equally to this work.

²To whom correspondence may be addressed. Email: qimingw@usc.edu, nicfang@mit.edu, or daraio@caltech.edu.

This article contains supporting information online at <https://www.pnas.org/lookup/suppl/doi:10.1073/pnas.2016524118/-DCSupplemental>.

Published January 11, 2021.

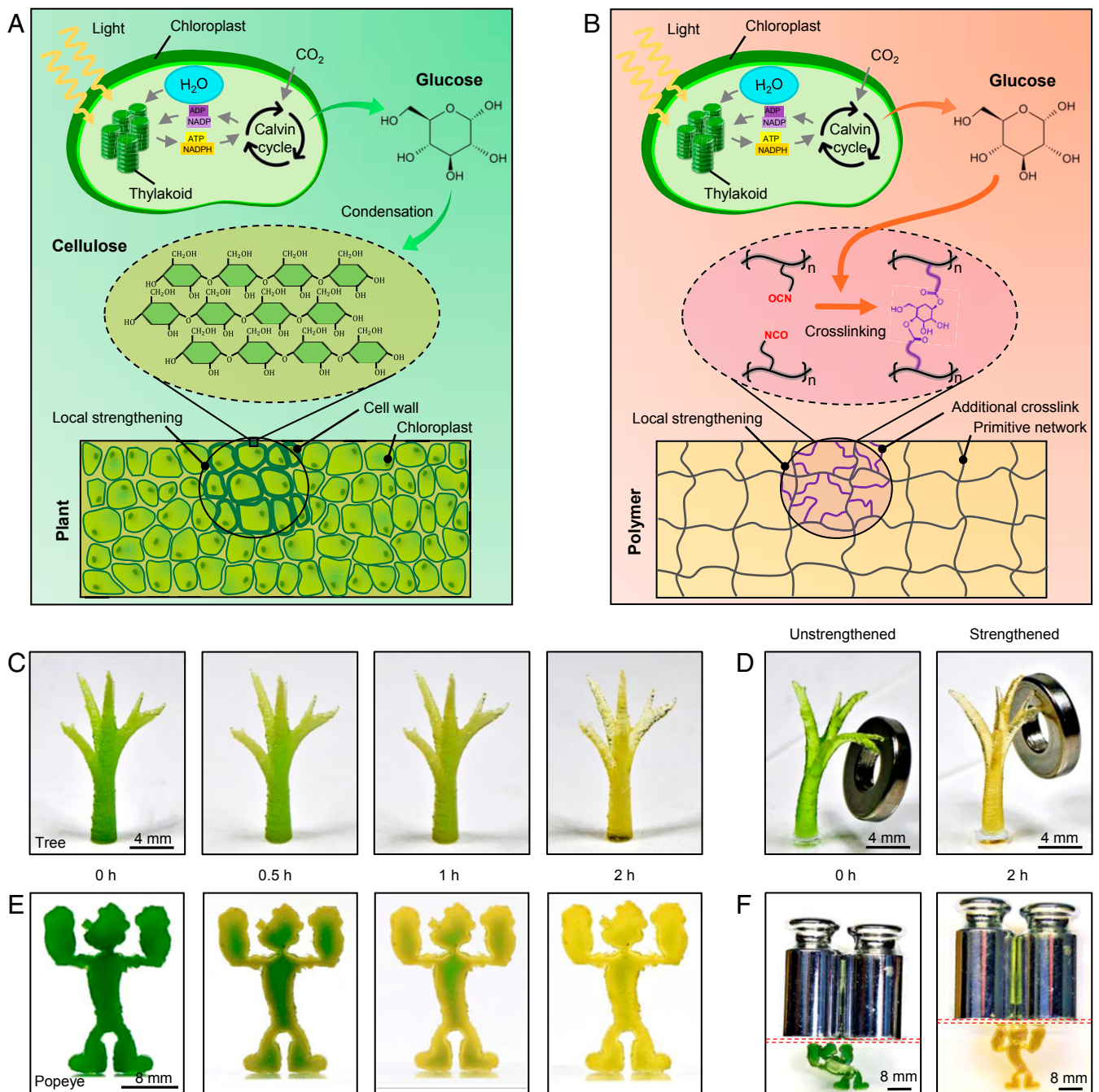


Fig. 1. Concept of the photosynthesis-assisted remodeling of 3D-printed structures. (A) Schematics to illustrate photosynthesis-assisted remodeling of plants. The photosynthesis-produced glucose undergoes a condensation reaction to form stiff polysaccharide (e.g., cellulose). (B) Schematics to illustrate photosynthesis-assisted remodeling of a synthetic polymer. The photosynthesis-produced glucose undergoes a reaction with isocyanate (NCO) side groups to form additional cross-links. (C) Image sequence of a 3D-printed treelike structure with various light illumination periods (white light intensity 69.3 W/m^2) of the photosynthesis process. (D) Unstrengthened and strengthened 3D-printed treelike structures loaded by the same weight (1 g). (E) Image sequence of a 3D-printed Popeye-like structure with various light illumination periods of the photosynthesis process. (F) Unstrengthened and strengthened 3D-printed Popeye-like structures loaded by the same weight (200 g). The red dashed boxes denote glass slides. The unstrengthened Popeye's height reduces by 34.7%, but the strengthened Popeye only by 7% (*SI Appendix, Fig. S7*).

low as $\sim 25 \mu\text{m}$. After the 3D-printing process, the NCO groups become free side groups within the polymer matrix (*SI Appendix, Fig. S4*). The NCO groups can enable a relatively strong reaction with hydroxyl groups (OH) on a glucose molecule to form urethane linkages ($-\text{NH}-\text{CO}-\text{O}-$) (Fig. 1B and *SI Appendix, Fig. S4*) (14). Since a glucose molecule has multiple OH groups, it is hypothesized that the OH groups on the chloroplast-produced

glucose can bridge multiple NCO groups to create new cross-links additional to the acrylate-enabled cross-links within the polymer matrix (Fig. 1B and *SI Appendix, Fig. S4*). Such additional cross-links are expected to significantly enhance the modulus and strength of the polymer (15, 16).

To demonstrate the strengthening concept, we 3D-print a treelike structure whose Young's modulus and tensile strength

gradually increase as the photosynthesis illumination period increases (white light intensity 69.3 W/m^2 , Fig. 1C and *SI Appendix*, Fig. S5). The strengthened structure with 2-h illumination shows a better weight-sustaining capability than the unstrengthened structure (Fig. 1D and *SI Appendix*, Fig. S6). Note that the photosynthesis process includes 2-h illumination of white light for glucose generation plus 2-h darkness for glucose exportation from the chloroplast (11, 17, 18). As an educational example, we 3D-print Popeye the Sailor, an American cartoon character who can strengthen his muscles by eating spinach (Fig. 1E). We show that the 3D-printed Popeye-like structure strengthens upon light exposure, by leveraging the photosynthesis process of the embedded spinach chloroplasts (2-h illumination and 2-h darkness). We demonstrate the strengthening effect by showing a reduced deformation upon loading (Fig. 1F and *SI Appendix*, Fig. S7).

We follow three steps to verify the hypothesized mechanism of photosynthesis-assisted strengthening (Fig. 2). In step 1, we verify that both light and chloroplasts are required to strengthen the designed polymer. We study three sample groups for comparison: The experimental group includes polymer samples with free NCO groups and embedded chloroplasts, going through 4-h illumination and 4-h darkness (Fig. 2A). To verify the effect of light, we employ control 1 group that includes polymer samples with free NCO groups and embedded chloroplasts, going through 8-h darkness (Fig. 2B). To verify the effect of chloroplasts, we employ control 2 group that includes polymer samples with free NCO groups but without chloroplasts, going through 4-h light illumination and 4-h darkness (Fig. 2C). We present the differences among these groups in three aspects. First, from the sample color, the initially green experimental samples turn to pale yellow, because light illumination can transform green chlorophyll to yellow lutein (Fig. 2D) (19). In contrast, control 1 and 2 samples remain green and semitransparent, respectively (Fig. 2E and F). Second, since the photosynthesis-produced glucose is expected to consume free NCO groups to form additional cross-links, the concentration reduction of free NCO groups can reveal the occurrence of the cross-linking reaction. To indicate the concentration of free NCO groups within the polymer matrix, we employ a Fourier transform infrared (FTIR) spectrometer to measure the transmittance of the sample around $2,260 \text{ cm}^{-1}$ that is corresponding to the NCO bond-stretching vibration (13). We find an evident peak at $2,260 \text{ cm}^{-1}$ in the initial state of all three sample groups (Fig. 2D–F). After the respective processes, the peak of the experimental group drastically drops, indicating the decreasing of the NCO concentration (Fig. 2D and *SI Appendix*, Fig. S8A); however, the peaks of controls 1 and 2 remain almost the same (Fig. 2E and F and *SI Appendix*, Fig. S8B and C). Third, we compare the mechanical properties of three sample groups via uniaxial tensile tests (Fig. 2G). Compared to controls 1 and 2, the experimental group exhibits higher Young's modulus and tensile strength by factors of 620 and 350%, respectively (Fig. 2H and *SI Appendix*, Fig. S9A). Since the strengthening is due to the formation of additional permanent covalent cross-links, the strengthened Young's modulus and tensile strength do not degrade within at least 6 mo (*SI Appendix*, Fig. S10). We further find that the fracture energy of the experimental sample is almost three times those of controls 1 and 2 (Fig. 2H and *SI Appendix*, Figs. S9B and S11) (20, 21). The toughening mechanism is similar to that in particle-reinforce composites, because the regions around chloroplast fillers are strengthened by forming new cross-links.

Note that the required water for the photosynthesis process is supplied by the water storage within the chloroplasts (17, 18), and the required carbon dioxide is supplied by the existing carbon dioxide within the matrix and diffusion from the atmosphere (22). A rough estimation shows these supplies of water and

carbon dioxide are sufficient for the experiments (*SI Appendix*, Table S1).

In step 2, we verify that chloroplasts can generate and export glucose to the polymer matrix. To detect the exported glucose within the polymer matrix, we employ a polymer sample with embedded chloroplasts but without free NCO groups (*SI Appendix*, Fig. S12). FTIR spectra show that the concentration of the OH group ($3,300\text{--}3,500 \text{ cm}^{-1}$) (23) increases in the matrix after the photosynthesis process, implying the existence of free glucose that is not consumed by NCO groups (*SI Appendix*, Fig. S13).

In step 3, we verify that glucose can directly strengthen the designed polymer with free NCO groups but without chloroplasts. FTIR spectra show that the peak for the NCO groups disappears when glucose concentration is sufficiently high (e.g., 0.398 M), indicating that the glucose completely consumes the free NCO groups (*SI Appendix*, Fig. S14). Tensile tests show that both Young's moduli and tensile strengths increase as the glucose concentration increases (*SI Appendix*, Fig. S15).

Next, we study the effects of two vital factors on the strengthening performance: concentration of embedded chloroplasts and light illumination period (Fig. 2I and J). First, we investigate polymer samples with chloroplasts of various weight concentrations (0–7 wt %) and free NCO groups (processed with 4-h illumination and 4-h darkness). Tensile stress–strain curves show that both Young's moduli and tensile strengths first increase with increasing chloroplast concentrations over 0–5 wt %, and then decrease afterward (5–7 wt %) (Fig. 2I and *SI Appendix*, Fig. S16A). The decrease after 5 wt % is probably because the chloroplasts serve as soft fillers within the polymer matrix, and a high concentration of soft fillers compromises the mechanical properties of the chloroplast-embedded polymer. Second, we employ various light illumination periods (white-light intensity 69.3 W/m^2) to process the polymer samples with 5 wt % chloroplasts and free NCO groups. Tensile stress–strain curves show that both Young's moduli and tensile strengths first increase (or reach a plateau) with increasing illumination time within 0–4 h, and then decrease afterward (4–6 h) (Fig. 2J and *SI Appendix*, Fig. S16B). The decrease after 4 h is probably because extralong illumination time may degrade the chloroplasts, associated with a reduction of the exported glucose concentration within the polymer matrix (similar behaviors for both 5 wt % (Fig. 2J) and 7 wt % of chloroplasts (*SI Appendix*, Fig. S16C)) (17, 18). Note that the effects of the chloroplast concentration and illumination period can be quantitatively explained by a theory that models the free energy of polymer networks with additional cross-links (*SI Appendix*, Figs. S17–S22 and Table S2).

A key difference between the presented hybrid synthetic-living material and the existing synthetic material is that the material property can be modulated by tuning the living activity of the involved biological element (i.e., chloroplast). Here, we employ a chilling temperature (0–4 °C) to temporarily freeze the activity of the embedded chloroplasts (24), and thus the material remains at the soft state after 2-h illumination and 2-h darkness (Fig. 2K and *SI Appendix*, Fig. S23 A–C). Once the temperature returns to 25 °C, the material can be strengthened to the stiff state via the photosynthesis process. This temporary freezing behavior cannot be achieved using traditional photoresins without living elements (*SI Appendix*, Fig. S23 D–F).

Another interesting feature of the presented material is that the photosynthesis-assisted strengthening can be reversed by cleaving the glucose cross-linkers with periodic acids (Fig. 2L and *SI Appendix*, Fig. S24) (25). With 2 M periodic acid, the Young's modulus and tensile strength of the initially strengthened polymer (with 4-h illumination and 4-h darkness) are reduced by 61 and 51%, respectively.

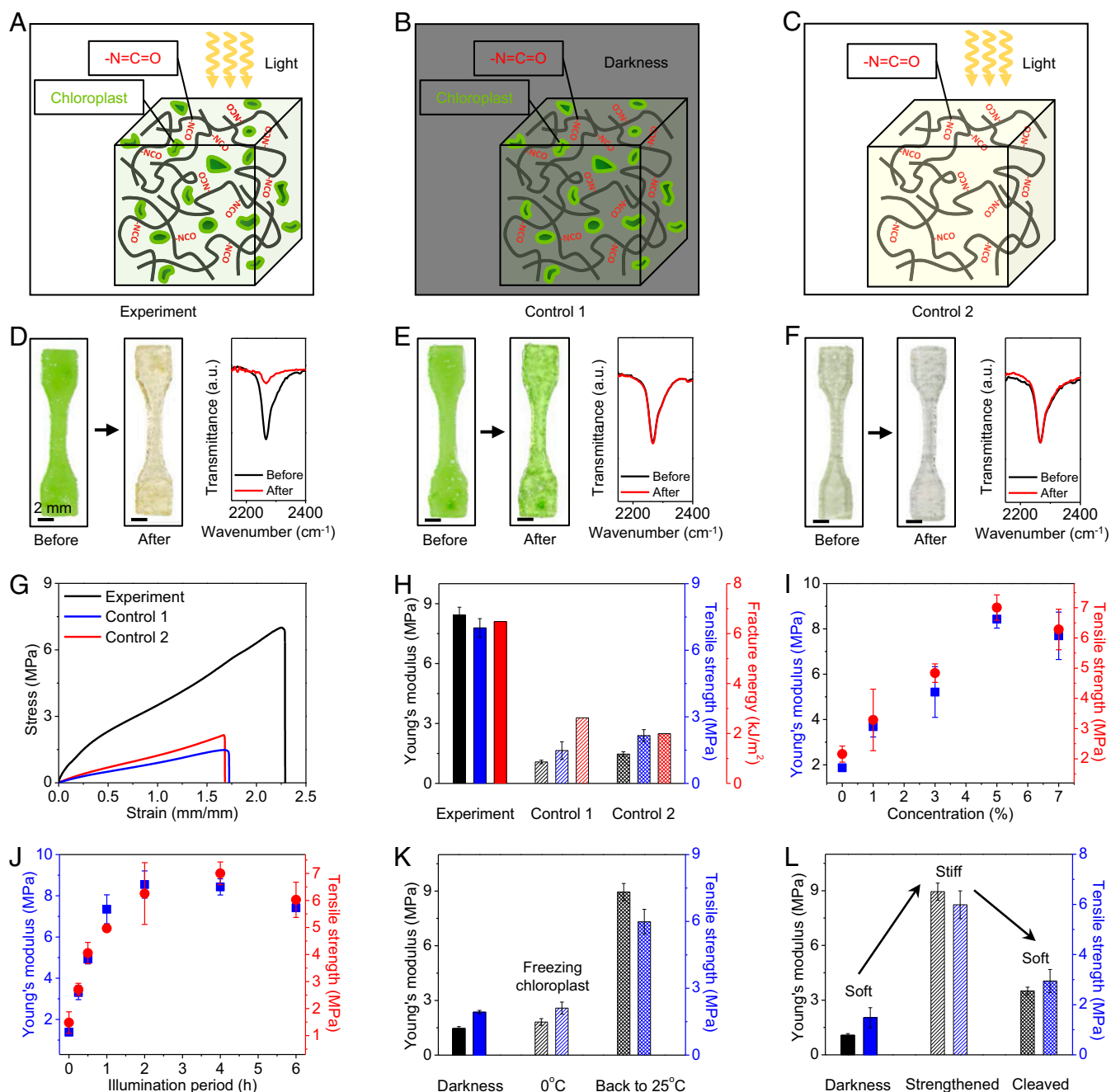
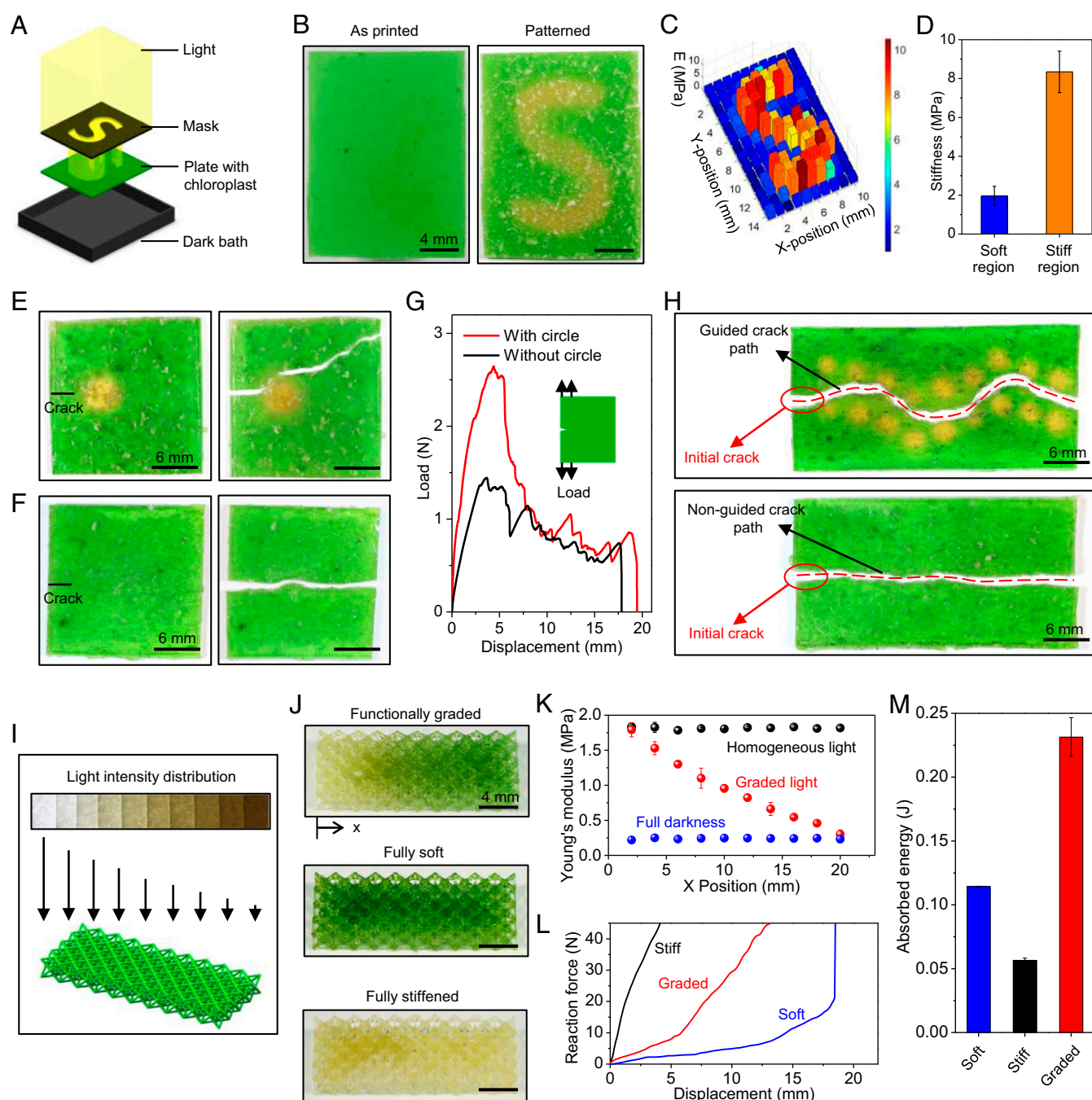


Fig. 2. Mechanism of photosynthesis-assisted strengthening. (A) Schematic of an experimental sample with free NCO groups and embedded chloroplasts undergoing 4-h light illumination and 4-h darkness. (B) Schematic of a control 1 sample with free NCO groups and embedded chloroplasts undergoing 8-h darkness. (C) Schematic of a control 2 sample with free NCO groups but without chloroplasts undergoing 4-h light illumination and 4-h darkness. (D–F) Samples and FTIR spectra before and after respective processes for (D) experiment, (E) control 1, and (F) control 2 cases, respectively. (G) Uniaxial tensile stress–strain curves of three groups of samples. (H) Young’s moduli, tensile strengths, and fracture toughnesses of three groups of samples. (I) Young’s moduli and tensile strengths of experimental samples of various weight concentrations (processed with 4-h illumination and 4-h darkness). (J) Young’s moduli and tensile strengths of experimental samples with 5 wt % chloroplasts after the photosynthesis processes with various light illumination periods. (K) Young’s moduli and tensile strengths of the processed experimental samples at three states: after 4-h darkness, after 2-h light and 2-h darkness at 0 °C, and after 2-h light and 2-h darkness at 0 °C followed by 2-h light and 2-h darkness at 25 °C. (L) Young’s moduli and tensile strengths of processed experimental samples at three states: after 8-h darkness, strengthened with 4-h light illumination and 4-h darkness, and strengthened and treated with 2 M HIO₄ solution to cleave the glucose cross-linkers. Error bars in H–L represent SDs of 3–5 samples.

Photosynthesis-Assisted Strengthening with Patterned Light

Next, we show that the photosynthesis-assisted strengthening can be tuned by patterned light (Fig. 3). We demonstrate localized strengthening by exposing a plate sample to a patterned light with an “S” shape (Fig. 3A). After the photosynthesis with 4-h illumination

and 4-h darkness, the illuminated S-shaped region turns from green to pale yellow (Fig. 3B and *SI Appendix*, Fig. S25). Indentation tests show that the average stiffness of the strengthened region is around 4.3 times that of the unstrengthened region (Fig. 3C and D and *SI Appendix*, Fig. S26). This local strengthening capability can be



ENGINEERING

Fig. 3. Photosynthesis-assisted strengthening with patterned light. (A) Schematic of an experimental setup for the localized strengthening through a patterned light with an S shape. (B) Samples at the as-printed state and after 4-h illumination with an S-shaped light and 4-h darkness. (C) Young's modulus distribution of the patterned sample measured with indentation tests. (D) Average stiffness of the unstrengthened and strengthened regions. (E) Crack detouring in a plate sample with a strengthened circle. (F) Straight crack in a plate sample without a strengthened circle. (G) Load-displacement curves of samples with and without the strengthened circle. (Inset) The loading setup. (H) Crack paths of samples with and without wavy strengthened regions. (I) Schematic to illustrate a 3D-printed lattice structure processed by a graded light (Left to Right: 69.3–0 W/m²). (J) Samples of functionally graded, fully soft, and fully stiffened lattices. (K) Effective Young's modulus distribution of three samples measured with indentation tests. (L) Compressive force-displacement curves of three samples with a loading rate of 10 mm/s. The loading is along the longitudinal gradient direction (x direction). (M) The absorbed energy of the three samples. The error bars in D and M represent SDs of 3–5 samples. Note that the inhomogeneous green color in E, F, and H is possibly due to some clusters of broken chloroplasts produced during the extraction experiments, which do not influence the result quality.

harnessed to detour crack paths within the material (Fig. 3 E–H). Due to the higher fracture toughness in the strengthened region, an initially straight crack detours a strengthened circle. The load-displacement curve shows that the toughness of the material is enhanced by 30% when a strengthened circle is installed (Fig. 3G). In

addition, judiciously patterning the strengthened regions can guide the crack to follow a wavy path, while the crack path in the virgin material is almost a straight line (Fig. 3H).

Photosynthesis can also be harnessed to strengthen 3D-printed structures. Similar to the treelike and Popeye-like structures in

Fig. 1 C–F, homogeneous light illumination can strengthen an Octet lattice to sustain a weight that is 830 times the lattice’s own weight, without buckling the beams (SI Appendix, Fig. S27). In contrast, the unstrengthened lattice is significantly buckled by the same weight. This strengthening mechanism can further be used to fabricate lattices with a graded stiffness (Fig. 3 I–M). Creating materials with graded functional properties has been a long-standing challenge in 3D-printed materials, because grading properties requires continuously switching printing inks during fabrication (26). Here, we expose an initially homogenous Octet lattice to a light pattern with graded intensity, to impart a gradient in stiffness (Fig. 3I and SI Appendix, Fig. S28). This is because higher illumination doses lead to higher stiffness within a certain illumination dose range (Fig. 2J). The functionally

graded lattice assumes a pale-yellow color at one end and remains green at the other end (Fig. 3J and SI Appendix, Fig. S29). We compare the results with two control samples, one stored in a dark environment for 8 h (fully soft, green lattice) and the other exposed to 4 h of homogeneous light illumination and 4-h darkness (fully stiffened, pale-yellow lattice). Indentation tests show that the effective Young’s modulus of the graded lattice decreases from 1.7 MPa at one end to 0.3 MPa at the other end (Fig. 3K). We apply a compressive load to the lattice with a relatively high loading rate (10 mm/s, Fig. 3L) and find that the absorbed energy in the graded lattice is around 1.7 times that of the soft lattice and 3.3 times that of the fully stiffened lattice (Fig. 3M).

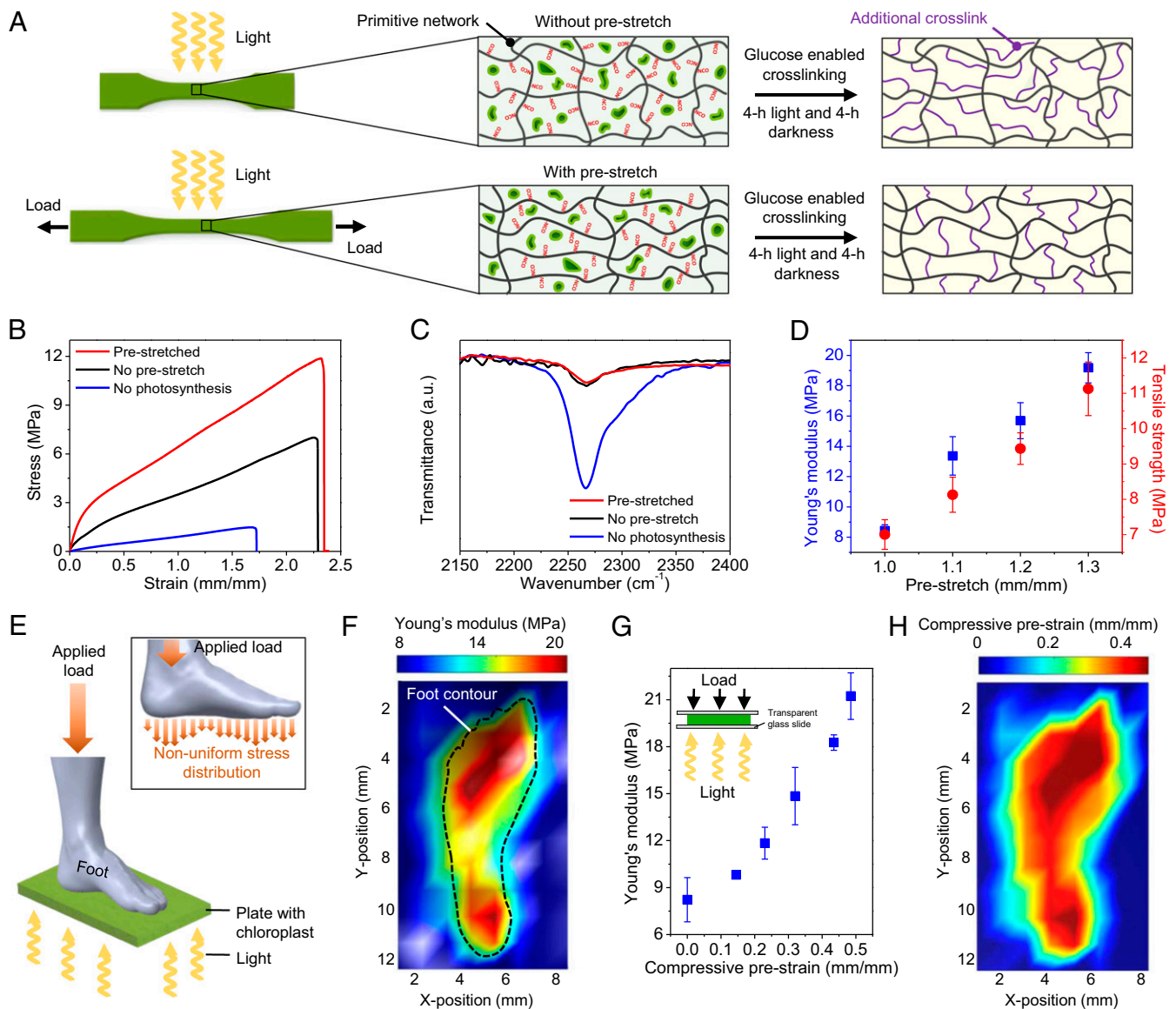


Fig. 4. Photosynthesis-assisted strengthening regulated by preloads. (A) Schematics to illustrate the photosynthesis-assisted strengthening in experimental samples without and with a prestretch. (B) Stress-strain curves of three samples: with a prestretch of 1.3 after 4-h light illumination and 4-h darkness, without a prestretch after 4-h light illumination and 4-h darkness, and without a prestretch after 8-h darkness. (C) FTIR spectra corresponding to the above three processed samples. (D) Young’s moduli and tensile strengths of the processed samples with various prestretches. Error bars represent SDs of 3–5 samples. (E) Schematics to illustrate the photosynthesis process on a sample plate under nonuniform prestresses applied by a 3D-printed foot. (F) Young’s modulus distribution of the processed sample plate. (G) The master curve between the applied compressive prestrain and the resultant Young’s modulus of the sample after the photosynthesis process (4-h illumination and 4-h darkness). Error bars represent SDs of 3–5 samples. (H) The compressive prestrain distribution translated from the Young’s modulus distribution in (F).

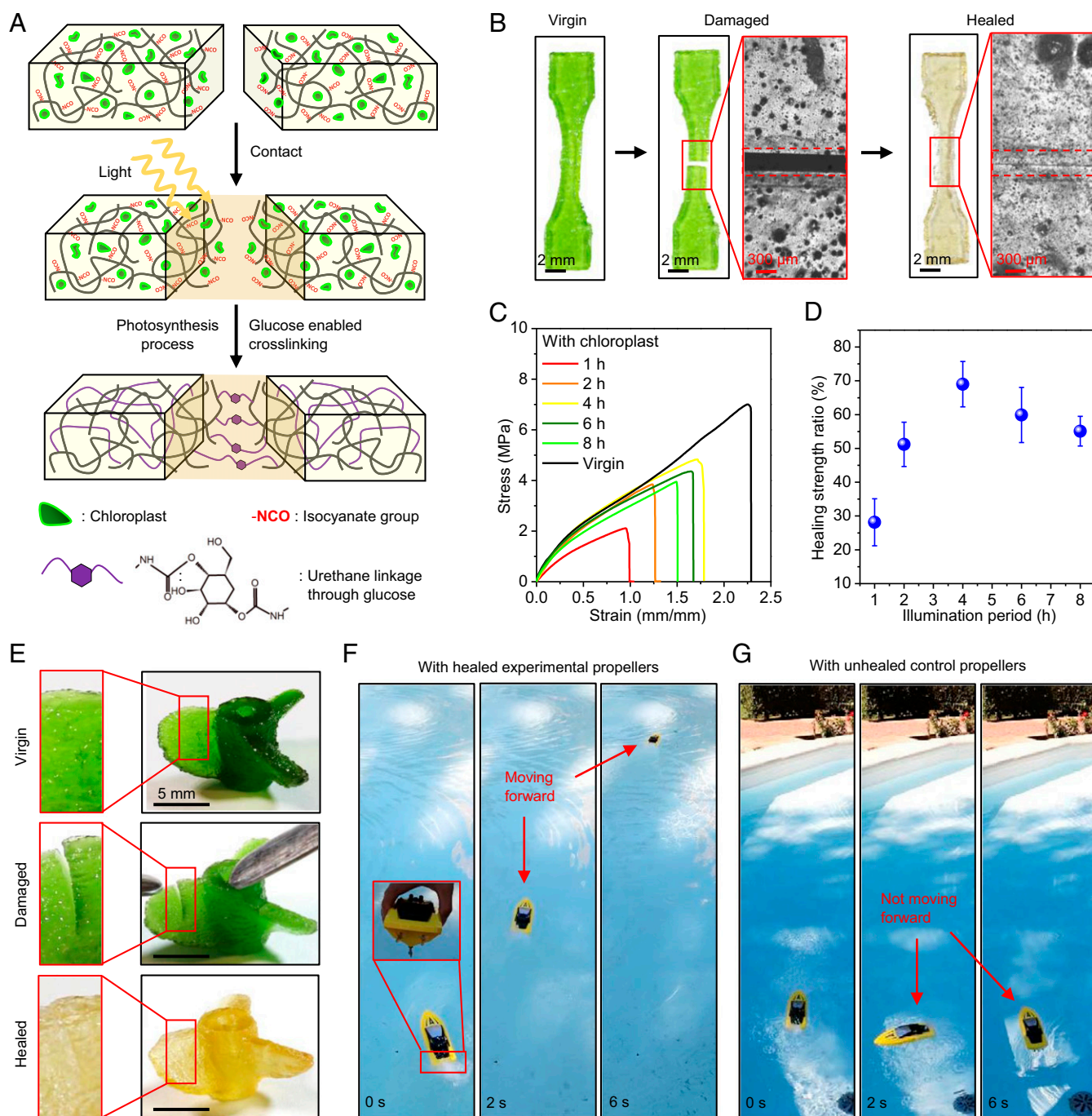


Fig. 5. Photosynthesis-assisted healing. (A) Schematic of photosynthesis-assisted healing of a fractured polymer through forming additional cross-links between free NCO groups and photosynthesis-produced glucose around the fracture surface. (B) Samples and interfacial microscope images at the virgin, damaged, and healed states. The healing process consists of 4-h light illumination and 4-h darkness. (C) Uniaxial tensile stress-strain curves of samples with various periods of light illumination time compared with that of the virgin sample. The virgin sample went through the photosynthesis process with 4-h light illumination and 4-h darkness. (D) Healing strength ratios of healed samples for various illumination periods. The healing strength ratio is defined as the tensile strength of the healed polymer normalized by that of the virgin sample. The error bars represent SDs of 3–5 samples. (E) Three-dimensional-printed experimental propeller structure at the virgin, damaged, and healed state. (Insets) Crack regions on a sector wing. (F) The healed experimental propellers assembled on a remotely controlled boat can facilitate the forward movement. (G) The unhealed propellers made of control 2 polymer ink (with free NCO groups but without chloroplasts) assembled on a remotely controlled boat cannot facilitate the forward movement.

Photosynthesis-Assisted Strengthening Regulated by Preloads

Mechanical loads can regulate plant remodeling through mechanotransduction pathways, to achieve higher stiffness and strength than those without the mechanical loads (5). Inspired by

plants, we here show that the photosynthesis-assisted strengthening of the experimental polymer can be regulated by mechanical preloads (Fig. 4A). We apply a prestretch to a sample, followed by a photosynthesis process (4-h illumination and 4-h darkness). The processed sample with a prestretch of 1.3 shows

higher Young's modulus and tensile strength by factors of 228 and 159%, respectively, compared to those without a prestretch (Fig. 4B). The enhancement of Young's modulus and tensile strength is not due to the density increase of additional cross-links, because FTIR spectra reveal that the density of additional cross-links in the processed prestretched sample is almost the same as that without a prestretch (Fig. 4C). We hypothesize that the enhancement is probably attributed to the architecture change of the additional cross-links corresponding to the deformation of the primitive network (Fig. 4A), because the formation of additional cross-links is based on the side chains with NCO groups. Further experiments show that Young's moduli and tensile strengths of the processed samples increase with increasing prestretches (Fig. 4D and *SI Appendix, Fig. S30*). This mechanism can be harnessed to realize a nonuniform stiffness distribution with nonuniform prestresses. For example, we apply nonuniform prestresses on a sample plate with a 3D-printed foot, and then illuminate light to enable the photosynthesis process (Fig. 4E). Indentation tests reveal an inhomogeneous stiffness distribution on the sample (Fig. 4F). To translate the stiffness mapping to a prestrain mapping, we need to obtain a master curve between a homogeneous compressive prestrain on a sample disk and the resultant stiffness of the sample after the photosynthesis process (4-h illumination and 4-h darkness) (Fig. 4G). With such a master curve, a prestrain mapping (Fig. 4H) can be translated from the stiffness mapping in Fig. 4F. The demonstrated function may facilitate the design of future customized footwear by fabricating shoe soles with an inhomogeneous stiffness distribution that is corresponding to the inhomogeneous stress distribution applied by the foot.

Note that the postcuring of a partially cured photoresin can enhance the stiffness (27, 28). However, the mechanism of forming additional cross-links is drastically different from that in the current work, because the postcuring is based on the free monomers that are typically not connected to the primitive network (*SI Appendix, Fig. S31A*). Thus, the prestretch of the primitive network would have a negligible effect on the architecture of additional cross-links. Experiments show that prestretch can hardly regulate the stiffness and strength of the postcured polymer (*SI Appendix, Fig. S31 B–D*).

Photosynthesis-Assisted Healing

Some plants exhibit outstanding healing capability during grafting and wound repairing (29, 30). Inspired by plants, we here show that photosynthesis can assist the healing of a fractured polymer sample by forming additional cross-links between free NCO groups and photosynthesis-produced glucose at the fracture surfaces (Fig. 5A). To demonstrate the healing process, we 3D-print a dumbbell-shaped sample with free NCO groups and embedded chloroplasts, cut it into two parts, and then bring the two parts into contact (Fig. 5B and *Movie S1*). After 4-h illumination and 4-h darkness, the fractured sample is healed with a smooth healing interface, verified by a microscopic image around the interface (Fig. 5B). The healed sample can be stretched up to 1.8 times of original length without breaking (*SI Appendix, Fig. S32* and *Movie S1*). To quantify the healing performance, we measure the tensile stress–strain behaviors of the healed samples after the photosynthesis process with different illumination periods (Fig. 5C). We find that the tensile strength ratio (tensile strength of the healed sample normalized by that of the virgin sample) increases with increasing illumination periods within 0–4 h and then decrease afterward (4–8 h) (Fig. 5D). The healing strength ratio for 4-h illumination can reach as high as $70 \pm 7\%$.

The decrease of the healing strength ratio after 4 h is probably because extralong illumination periods may degrade the chloroplasts, associated with the reduction of the exported glucose concentration (17, 18). As a contrast, the control 2 polymer with free NCO groups but without embedded chloroplasts exhibits a poor healing performance with the healing strength ratio as low as 9% (*SI Appendix, Fig. S33A*). The microscopic image shows that the contacted fracture interface still leaves an evident gap after 4-h illumination and 4-h darkness (*SI Appendix, Fig. S33B*).

The photosynthesis-assisted healing mechanism can be harnessed to repair a propeller 3D-printed with the experimental polymer ink (Fig. 5E–G). A crack is installed on each wing of the propeller, and these cracks can be healed after the photosynthesis process (4-h illumination and 4-h darkness, Fig. 5E). On the contrary, cracks on the wings of a propeller 3D-printed with the control 2 polymer ink cannot be healed with the illumination process (*SI Appendix, Fig. S34*). To demonstrate the performance, the healed experimental propeller that assembled on a remotely controlled boat can facilitate the forward movement of the boat (Fig. 5F and *Movie S2*). However, the unhealed control propellers cannot push the boat forward due to the lack of enough propulsion force (Fig. 5G and *Movie S2*).

Conclusion

We harness photosynthesis in chloroplasts embedded in a synthetic polymer matrix to remodel 3D-printed structures and demonstrate matrix strengthening and crack healing. While the field of engineered photosynthesis shows a promising capability in producing energy fuels (31, 32), the current work extends the concept to advanced materials, by introducing a downstream reaction mechanism to use the photosynthesis-produced glucose. Besides, the presented photocurable polymers can be used in various photopolymerization-based 3D-printing systems, such as stereolithography (12, 13), polyjet (26), photopolymer waveguides (33), two-photon lithography (7, 34), continuous liquid production (35), and volumetric lithography (36, 37). To this end, the communication between living photosynthesis and synthetic 3D-printable polymers may open doors for hybrid synthetic-living materials with both complex architectures and biomimetic properties.

In the future study, maintaining the long-term living states of chloroplasts or even regenerating chloroplasts is a very important aspect. One possible solution would be refreshing of living chloroplasts using a flow system (38), such as a microfluidic flow of chloroplasts through a porous material framework.

Materials and Methods

Living chloroplasts were extracted from fresh baby spinach leaves (*Spinacia oleracea* L.). To fabricate polymer inks with free NCO groups, 0.02 mol of isophorone diisocyanate, 10 wt % of dimethylacetamide, and 1 wt % of dibutyltin dilaurate were mixed with the preheated Poly(tetrahydrofuran) (average molar mass 650 g/mol) at 70 °C and stirred with a magnetic stir bar for 1 h. After reducing the temperature to 40 °C, 0.01 mol of 2-Hydroxyethyl methacrylate was added and mixed for 1 h. Then, extracted chloroplasts (0–7 wt %) and 2 wt % of photoinitiator (phenylbis(2,4,6-trimethylbenzoyl)phosphine oxide) were gently mixed with the prepared polymer inks using a magnetic stir bar for 30 min at 5 °C in a dark environment. Subsequently, the polymer samples were 3D-printed with a bottom-up stereolithography system. Detailed descriptions of the experimental procedures and theoretical modeling are provided in *SI Appendix*.

Data Availability. All study data are included in the article and *SI Appendix*.

ACKNOWLEDGMENTS. Q.W. acknowledges the funding support from the Air Force Office of Scientific Research (Grant FA9550-18-1-0192, program manager: Dr. Ming-Jen Pan) and the NSF (Grants CMMI-1762567 and CMMI-1943598).

1. D. Barthélémy, Y. Caraglio, Plant architecture: A dynamic, multilevel and comprehensive approach to plant form, structure and ontogeny. *Ann. Bot.* **99**, 375–407 (2007).
2. Z. A. Popper *et al.*, Evolution and diversity of plant cell walls: From algae to flowering plants. *Annu. Rev. Plant Biol.* **62**, 567–590 (2011).

3. M. Ashby, "The CES EduPack database of natural and man-made materials" (Cambridge University and Granta Design, Cambridge, UK, 2008).
4. D. U. Shah, T. P. S. Reynolds, M. H. Ramage, The strength of plants: Theory and experimental methods to measure the mechanical properties of stems. *J. Exp. Bot.* **68**, 4497–4516 (2017).

5. A. Sampathkumar, A. Yan, P. Krupinski, E. M. Meyerowitz, Physical forces regulate plant development and morphogenesis. *Curr. Biol.* **24**, R475–R483 (2014).
6. R. L. Truby, J. A. Lewis, Printing soft matter in three dimensions. *Nature* **540**, 371–378 (2016).
7. J. Bauer *et al.*, Nanolattices: An emerging class of mechanical metamaterials. *Adv. Mater.* **29**, 1701850 (2017).
8. Y. Yang *et al.*, Recent progress in biomimetic additive manufacturing technology: From materials to functional structures. *Adv. Mater.* **30**, e1706539 (2018).
9. M. Kadic, G. W. Milton, M. van Hecke, M. Wegener, 3D metamaterials. *Nat. Rev. Phys.* **1**, 198–210 (2019).
10. J. U. Surjadi *et al.*, Mechanical metamaterials and their engineering applications. *Adv. Eng. Mater.* **21**, 1800864 (2019).
11. D. Joly, R. Carpentier, "Rapid isolation of intact chloroplasts from spinach leaves" in *Photosynthesis Research Protocols*, R. Carpentier, Ed. (Humana Press, 2011), vol. 684, pp. 321–325.
12. Q. Wang *et al.*, Lightweight mechanical metamaterials with tunable negative thermal expansion. *Phys. Rev. Lett.* **117**, 175901 (2016).
13. K. Yu *et al.*, Healable, memorizable, and transformable lattice structures made of stiff polymers. *NPG Asia Mater.* **12**, 26 (2020).
14. J.-Y. Zhang *et al.*, Synthesis, biodegradability, and biocompatibility of lysine diisocyanate-glucose polymers. *Tissue Eng.* **8**, 771–785 (2002).
15. A. L. B. Ramirez *et al.*, Mechanochemical strengthening of a synthetic polymer in response to typically destructive shear forces. *Nat. Chem.* **5**, 757–761 (2013).
16. T. Matsuda, R. Kawakami, R. Namba, T. Nakajima, J. P. Gong, Mechanoresponsive self-growing hydrogels inspired by muscle training. *Science* **363**, 504–508 (2019).
17. D. W. Lawlor, *Photosynthesis: Molecular, Physiological and Environmental Processes* (Longman Scientific & Technical, 1993).
18. R. P. F. Gregory, *Biochemistry of Photosynthesis* (Wiley, London, 1977), vol. 5.
19. K. Okada, Y. Inoue, K. Satoh, S. Katoh, Effects of light on degradation of chlorophyll and proteins during senescence of detached rice leaves. *Plant Cell Physiol.* **33**, 1183–1191 (1992).
20. R. Rivlin, A. G. Thomas, Rupture of rubber. I. Characteristic energy for tearing. *J. Polym. Sci.* **10**, 291–318 (1953).
21. J.-Y. Sun *et al.*, Highly stretchable and tough hydrogels. *Nature* **489**, 133–136 (2012).
22. H. Xiao, Z. H. Ping, J. W. Xie, T. Y. Yu, Permeation of CO₂ through polyurethane. *J. Appl. Polym. Sci.* **40**, 1131–1139 (1990).
23. M. V. Korolevich, R. G. Zhabankov, V. V. Sivchik, Calculation of absorption-band frequencies and intensities in the IR-spectrum of alpha-d-glucose in a cluster. *J. Mol. Struct.* **220**, 301–313 (1990).
24. X. Liu, Y. Zhou, J. Xiao, F. Bao, Effects of chilling on the structure, function and development of chloroplasts. *Front. Plant Sci.* **9**, 1715 (2018).
25. J. D. Rawn, R. J. Ouellette, *Organic Chemistry: Structure, Mechanism, Synthesis* (Academic Press, 2018).
26. N. W. Bartlett *et al.*, SOFT ROBOTICS. A 3D-printed, functionally graded soft robot powered by combustion. *Science* **349**, 161–165 (2015).
27. J. Rys, S. Steenhusen, C. Schumacher, C. Cronauer, C. Daraio, Locally addressable material properties in 3D micro-architectures. *Extreme Mech. Lett.* **28**, 31–36 (2019).
28. H. Yin, Y. Ding, Y. Zhai, W. Tan, X. Yin, Orthogonal programming of heterogeneous micro-mechano-environments and geometries in three-dimensional bio-stereolithography. *Nat. Commun.* **9**, 4096 (2018).
29. C. W. Melnyk, E. M. Meyerowitz, Plant grafting. *Curr. Biol.* **25**, R183–R188 (2015).
30. R. Bloch, Wound healing in higher plants. II. *Bot. Rev.* **18**, 655 (1952).
31. N. Kornienko, J. Z. Zhang, K. K. Sakimoto, P. Yang, E. Reisner, Interfacing nature's catalytic machinery with synthetic materials for semi-artificial photosynthesis. *Nat. Nanotechnol.* **13**, 890–899 (2018).
32. K. K. Sakimoto, N. Kornienko, P. Yang, Cyborgian material design for solar fuel production: The emerging photosynthetic biohybrid systems. *Acc. Chem. Res.* **50**, 476–481 (2017).
33. T. A. Schaedler *et al.*, Ultralight metallic microlattices. *Science* **334**, 962–965 (2011).
34. L. R. Meza, S. Das, J. R. Greer, Strong, lightweight, and recoverable three-dimensional ceramic nanolattices. *Science* **345**, 1322–1326 (2014).
35. J. R. Tumbleston *et al.*, Additive manufacturing. Continuous liquid interface production of 3D objects. *Science* **347**, 1349–1352 (2015).
36. M. Shusteff *et al.*, One-step volumetric additive manufacturing of complex polymer structures. *Sci. Adv.* **3**, eaao5496 (2017).
37. B. E. Kelly *et al.*, Volumetric additive manufacturing via tomographic reconstruction. *Science* **363**, 1075–1079 (2019).
38. T. E. Miller *et al.*, Light-powered CO₂ fixation in a chloroplast mimic with natural and synthetic parts. *Science* **368**, 649–654 (2020).